MAX-PLANCK-INSTITUT FÜR PLASMAPHYSIK

GARCHING BEI MÜNCHEN

A Single-Exposure Imaging Device for Infrared and Submillimeter Wavelength Laser Radiation

F. Keilmann

IPP IV/18 May 1971

Die nachstehende Arbeit wurde im Rahmen des Vertrages zwischen dem Max-Planck-Institut für Plasmaphysik und der Europäischen Atomgemeinschaft über die Zusammenarbeit auf dem Gebiete der Plasmaphysik durchgeführt.

IPP IV/18 F. Keilmann

A Single-Exposure Imaging Device for Infrared and Submillimeter Wavelength Laser Radiation

May 1971 (in English)

Abstract

A detector for two-dimensional observations of infrared and submillimeter wavelength radiation is described. It allowed mode structures and interference patterns to be imaged for the first time with the 337 /u radiation of an HCN-laser.

The image conversion effect is based firstly on radiation absorption by a metal film and secondly on temperature display presented by the colour shift in a liquid crystal layer. Irrespective of the wavelength of the infrared radiation, full contrast is achieved at the input energy density of o.oo4 J/cm^2. Single pictures can therefore be taken in short exposure times, viz. $1o^{-9}$ sec at a wavelength of 1o.6 /u (CO_2-laser) or $1o^{-5}$ sec at 337 /u (HCN-laser). A spatial resolution of 1oo line pairs per mm can be achieved if the exposure time is below $1o^{-4}$ sec, which calls for a power density of at least 4o W/cm^2.

Table of Contents

Introduction

For infrared light with wavelengths longer than about 2 μ there are no photographic films that allow imaging based on photochemical reactions. However, the long wavelength radiation from the infrared up to the submillimeter region is of particular interest in plasma diagnostics. Infrared radiation can act as a selective probe for measuring the electron density distribution since the refractive index at these wavelengths is mainly governed by the plasma electrons. The following is an outcome of detailed estimates /1/: There is a linear relation between the phase velocity and the electron density n_e, in the ranges $10^{12} \lesssim n_e \lesssim 10^{15}$ cm^{-3} for HCN-laser radiation (wavelength 0.337 mm) and $10^{15} \lesssim n_e \lesssim 10^{18}$ cm^{-3} for CO_2-laser radiation (wavelength 10.6 μ).

Besides this application in plasma physics, infrared photography is wanted for astronomy, geography, medicine, and material testing. Attempts are being made in these fields to record infrared radiation in order to pinpoint radiation sources or to determine two-dimensional distributions of temperature and emissivity. For this purpose infrared cameras have been built in which a quantum detector scans the image field point by point and displays it on a TV screen. This is done by rotating mirrors and prisms. In particular, the development of efficient and sophisticated image converters has been stimulated by military demand for air reconnaissance /2/.

In plasma diagnostics the time resolution required of an image detector is often much higher than can be achieved with rotating deflection systems since the state of the plasma may vary at time scales of 10^{-6} or 10^{-9} sec. In fact, quantum detectors with rise times of around 10^{-9} sec are available; many of these could be arranged in a mosaic for image conversion. As far as the author is aware, however, such an elaborate system has not yet been built.

With the advent of high power lasers in the infrared and submillimeter regions a different class of image converters has

become practicable, in which infrared radiation induces optically visible phenomena, particularly as a result of temperature dependent effects.

1. Thermal Image Converters

In thermal image converters the infrared radiation energy is converted to heat, so that a temperature pattern corresponding to the investigated infrared image appears in the absorbing layer. This is then made visible by a temperature dependent optical effect in the absorbing layer itself or in a second layer specially applied for the purpose.

A thermal image converter can therefore be of very simple design, unlike the scanning system above, but it is inferior to quantum detectors as regards rise time and, in particular, decay time. Fortunately, however, neither time constant is relevant in plasma diagnostics. What is important is that single pictures can be taken with sufficiently short exposure time.

For displaying the temperature image irreversible optical effects may be used. It is possible, for example, to induce or accelerate chemical reactions /3 - 6/. Heating may cause the substrate to melt /7/ or evaporate /8, 9/; it is surprising that despite its very good energy resolution of 10^{-5} J/cm^2 the evaporograph according to CZERNY has not been used hitherto to record infrared laser radiation.

Reversible effects have the advantage that the image converter returns by itself to the initial state after an exposure. For example, thermal expansion can be recorded by optical holography /10/. Heat-quenched phosphors /11, 12/ and cholesteric liquid crystals /13 - 17/ are, however, much more sensitive temperature indicators. In fact, a 0.04 μ thick film of such a phosphor is sufficient for observation, whereby a temperature difference of 0.05 $^{\circ}$C can be resolved. In spite of that, phosphors are less suitable for observing pulsed laser radiation. This is because the low luminous density of the fluorescence excited by ultra-

violet radiation would necessitate a much too long exposure time for read-out, about o.1 sec even with fast photographic films.

On the other hand, cholesteric liquid crystals do not have this disadvantage. The light intensity usable for read-out in this case is proportional to the white light intensity used for illumination, and so with flash-lamps read-out times of 1 msec and less are readily achieved. The image conversion effect here results from the back-scattered light having only one spectral component owing to Bragg interference; the wavelength of this component, i.e. the colour, shifts with the lattice structure of the liquid crystal on change of temperature. To achieve a sufficient scattering effect, an approximately lo μ thick liquid crystal layer (about 5o lattice planes) is required. If a substance whose working range covers 1.5 ^{o} C between red and blue is chosen, it is possible to resolve a temperature difference of about o.2 ^{o} C.

2. A Thin Film Absorber for Infrared and Submillimeter Radiation

To obtain the highest possible sensitivity in a thermal image converter, a large percentage of the radiation has to be absorbed. On the other hand, this must be done by a thin film since the temperature rise is inversely proportional to the heat capacity. This material problem mostly depends on the wavelength used. For example, with a 15o μ thick two-layer element of liquid crystal and Mylar /16/ the absorption at λ = lo.6 μ is 8o %, while at λ = 337 μ no absorption can be observed. This is also true of various other plastics that would be suitable as substrate foil for the liquid crystal film.

An ideal way to absorb radiation is to use an extremely thin metal layer /18, 19/. It can be made in such a way that in the spectral range of interest (λ = 1 μ up to radio wavelengths) it absorbs 5o %, irrespective of the wavelength; i.e., it behaves exactly like a half-black body. The necessary film thickness is less than o.1 μ. This means that it does not add significantly to the heat capacity of the displaying liquid crystal layer and of the approximately 2 - 5 μ thick base foil.

The absorption behaviour of a thin metal film can be followed from the complex refractive index /18/:

$$\hat{n} = (1 + i) \cdot \sqrt{\sigma / 2\omega\varepsilon_o}$$

where σ is the electrical conductivity, ω the frequency, and ε_o the vacuum dielectric constant. σ varies at visible light frequencies but is constant over the spectral region investigated. For the dependence of the absorption on the film thicknes Fresnel's equations yield a maximum between the extremes of complete transmission at $d \to 0$ and complete reflection at $d \to \infty$. The relevant film thickness for highly conducting metals is always very small compared to 1 /u and so for the spectral region investigated it holds that $\lambda \gg d$. Fresnel's equations thus become very simple. For vertical incidence with $f = \sigma \cdot d \cdot \sqrt{\mu_o / \varepsilon_o}$ one gets

$$R = \frac{f^2}{(2+f)^2}$$

$$T = \frac{f^2}{(2+f)^2}$$

$$A = \frac{4f}{(2+f)^2}$$

where R, T, and A denote the reflected, transmitted, and absorbed components respectively of the radiation power.

An absorption maximum A = o.5 is obtained for f = 2, and hence $1/\sigma \cdot d$ = 189 Ω. The term $1/\sigma \cdot d$ may be regarded as the resistance of a flat slab with square base area a^2 and height d; since it is independent of a, it may also be called surface resistance.

For the optimal surface resistance of 189 Ω the following film thicknesses are calculated: o.8 Å for silver, 5.4 Å for iron, and 9.2 Å for chromium, i.e. only few atomic layers. In actual fact the films have to be much thicker because the conductivity under these conditions is appreciably reduced by lattice defects.

Experimentally, an absorbing metal film was produced by vacuum depositing chromium on a 3 μ thick Hostaphan foil (Fig.1). First the foil is stretched on a plastic holder 14 cm in diameter. Two parallel strip electrodes are then mounted 7 cm apart. The square area intervening is then coated until the resistance drops to about 2oo Ω. It is not essential to get the value 189 Ω exactly because the above equations show that the absorption exceeds 4o % for resistances between 7o and 4oo Ω. By opening the vacuum vessel no change in surface resistance is observed. The coated surface appears dully reflecting (Fig.1).

An absorbing film with a surface resistance of 28o Ω was used to make absorption measurements by determining the transmission for vertical incidence and the reflection for nearly vertical incidence, the total error being $\pm$ 15 %. The radiation sources used were a HeNe-laser (wavelength o.63 μ), a Nd-laser (1.o6 μ), a CO_2-laser (1o.6 μ), an HCN-laser (337 μ), and an X-band klystron (3 cm). For this frequency range covering 15 octaves the absorption values were constant, between 35 and 55 % in agreement with theory.

The resistance does not change when the film is treated with solvents such as alcohol or petroleum ether. Crumpling the film, however, strongly increases the d.c. resistance since the metal cracks, but this does not affect the radiation absorption.

It is doubtful whether the thin metal foil would withstand the strain if used for observing very short, high power radiation pulses. Assuming the breakdown strength of the material to be $1o^5$ V/cm, radiation power densities up to 24 MW/cm^2 could be tolerated. To make a further estimate, we anticipate the sensitivity as discussed in the next section: An absorbed radiation energy density of o.oo15 J/cm^2 is required to achieve the full temperature contrast of o.5 ^oC, which corresponds to an input of approximately o.oo4 J/cm^2. From this now we find the shortest possible exposure time to be o.17 nsec. This allows a single 1 nsec mode-lock pulse from a transversely excited high pressure CO_2-laser to be used for imaging.

In addition, it has to be checked whether the metal foil can withstand the thermal stress. A maximum temperature rise occurs when the length of the radiation pulse is short relative to the characteristic time constant of the thermal conduction. With an absorbed energy of o.ool5 J/cm^2 the melting-point for chromium is reached when the film thickness is less than 28 Å (probably the actual thickness of our film is about 2o to 5o Å). A rough estimate of the heat flow is provided by the one-dimensional steady-state equation of thermal conduction:

$$\frac{Q}{\tau} = \lambda \cdot \frac{\Delta T}{\Delta x}$$

With a thermal conductivity $\lambda \approx$ o.oo2 W/cm °C (Hostaphan) this means that the thermal energy $Q = 10^{-3}$ J/cm^2 can flow away in τ = 1o nsec over a gradient of 5oo °C at a length of o.1 µ. So an experimental check would be useful to see whether the metal film is damaged at exposure times less than 1o nsec.

At all events there is definitely no damage at an exposure time of 3oo msec, as was observed with TEA-CO_2-laser pulses having a power density of 13 KW/cm^2 (field strength here 2ooo V/cm).

3. Transient Response of the Liquid Crystal Detector

The display in liquid crystal image converters is suitably achieved with substances whose working range at 35 °C is safely above room temperature, with a useful temperature range of 1.5 °C. The colours red, yellow, green, and blue than indicate temperatures of about 35, 35.5, 36, and 36.5 °C. Full contrast is thus achieved by a temperature rise of o.5 °C. The necessary quantity of heat is calculated to be o.ool5 J/cm^2 for the case where a 3 µ thick Hostaphan foil is coated on one side with a 3o Å thick chromium film and on the other with a 7 µ thick liquid crystal film.

In this section, only infrared exposure times less than o.1 sec will be considered. This ensures, as will be shown later, that heat transport mechanisms other than thermal conduction play no part in producing the colour image. Due to thermal conduction,

the energy of o.oo15 J/cm^2 localized at first near the metal film, propagates with a time constant which can again be estimated from the thermal conduction equation, to be about o.ooo3 sec (Q = o.oo1 J/cm^2, λ = o.oo2 W/cm ^oC, ΔT = 1 ^oC, Δx = 5 μ). It is therefore best to read out the temperature image with a delay of about o.5 msec. With longer delay the spatial resolution gets poorer. Possibly, some delay may have to be accepted as it is not sure at what rate the structural change of the liquid crystal follows the temperature rise.

As long as the spatial resolution is limited by thermal conduction effects, it can readily be estimated: if it is possible to read out after a delay of about o.ooo3 sec, intensity maxima should be clearly separable at a distance equal to the film thickness 1o μ. The detector can thus resolve 1oo line pairs per mm, provided that the infrared exposure time does not exceed $1o^{-4}$ sec, i.e., the infrared power does exceed 4o W/cm^2. If the radiation power is lower, a longer exposure time has to be chosen. How does the spatial resolution decrease with increasing exposure time?

For this case only the thermal conduction parallel to the film will be considered, and it is assumed that the infrared light bundle uniformly illuminates a spot of diameter D in a relatively short exposure time. The absorbed energy is then Q = o.oo15 J/cm^2 $\cdot$ $\pi \cdot (\frac{D}{2})^2$. Heat flows away through the boundary area of this spot F = 1o $\mu \cdot \pi \cdot$ D. What interests us is the time after which the excess temperature of o.5 ^oC begins to disappear in the center of the spot. The driving temperature gradient can be assumed to be o.5 ^oC/D. Irrespective of D, the linear thermal conduction equation yields for this state a heat flux

$$\frac{Q}{\tau} = \lambda \cdot F \cdot \frac{o.5\ ^oC}{D} = 3 \cdot 1o^{-6}\ W$$

where λ = o.oo2 W/cm^2 ^oC. Half of the originally absorbed energy then flows away in the time τ = 25o D^2 (τ in sec, D in cm). Thus, 1o μ large spots disappear in about o.ooo3 sec, but 1 mm spots take 3 sec. The following behaviour of the spatial resolution as a function of the exposure time can thus be given (order of magnitude):

Exposure time in sec	1	o.1	o.ol	o.ool	≤ o.oool
Resolvable line pairs per mm	1	3	1o	3o	1oo

It can be concluded from this that an exposure time of o.1 sec is completely sufficient for diffraction limited observation of HCN-laser radiation, which is equivalent to a power density of 4o mW/cm^2.

4. Stationary Images and Setting of Working Point

If an exposure time of 1 sec or longer has to be used to record an infrared image due to low power densities $\lesssim$ o.oo5 W/cm^2, the temperature balance is affected by convective heat losses and emission of radiation.

The emission L is equal to that of a blackbody into half-space because the foil has a broad-band absorption coefficient of o.5 and emits into full space. A small temperature rise ΔT at 3oo ^oK yields

$$\Delta L = o.oo06 \cdot \Delta T \quad W/cm^2$$

i.e., the emission from the illuminated areas is greater by o.ooo3 W/cm^2 than that from the surrounding region, if the latter is o.5 ^oC colder.

This shows that an absorbed signal power of as little as o.ooo3 W/cm^2 will just maintain a stationary "image" with ΔT = o.5 ^oC. For this limiting case, however, the required exposure time will be very long, and it is to be expected that the contrasts will drop below the observation limit owing to temperature equalization via thermal conduction.

Let us take instead an absorbed signal power fifty percent higher, i.e., o.ooo45 W/cm^2. The net power during image formation is then > o.oool5 W/cm^2, and so the exposure time needed to attain the net energy o.ool5 J/cm^2 is $\lesssim$ lo sec. The estimates in the previous section then state that even at this long exposure time spatial frequencies of 3 line pairs per cm give good contrast. If this spatial resolution is acceptable, the low radiation power density of o.ool W/cm is sufficient for image conversion.

Hitherto there has been no mention of convective heat transport. At an excess temperature of the liquid crystal film of lo ^{o}C relative to the ambient air the convective heat transport can be estimated as o.oo6 W/cm^2. Unlike the thermal radiation losses, these losses cannot be compensated by the heating mechanism, discussed later, in order to reach the operating temperature of 35 ^{o}C all over the sensitive area: the heated air moves near the surface and heats higher lying parts, resulting in a highly non-uniform temperature distribution.

Convective disturbances can obviously be avoided in two ways: either the air temperature is made 35 ^{o}C or the air is pumped off. The former would only be feasible in temperature-controlled rooms; closed vessels with temperature-controlled air are impracticable since the temperature of the indispensable thin polythene window, approximately 5o cm^2 in area, cannot be kept sufficiently constant; the interior is thus subject to air disturbances which cause the detector temperature to fluctuate by a few o.1 ^{o}C.

If, on the other hand, the air is pumped off to about 1 torr, it is possible to achieve uniform pre-heating. This does not affect the reaction of the liquid crystal. A constant working temperature can be achieved by uniform irradiation, for example, with an electrically heated metal plate.

Preheating by this method is not practical, however, for spatial reasons to be discussed in the next section. Instead, the thermal radiation from a heating ring /16/ can be used (see Fig.2). The input intensity I is then

$$I \sim \frac{1}{z_o} \cdot \int_o^{2\pi} \frac{d\varphi}{\sqrt{R^2 + z_o^2 + r^2 - 2\, r\, R \cos\varphi}}$$

The radiation profiles thus calculated (Fig.3) show that with a ring diameter of 7 cm an approximately uniform temperature distribution can be achieved if the distance is about 2 cm. Experimental confirmation was obtained. The heating system shown in Fig.4 has been successfully used under vacuum conditions. For the optimum distance of 2.7 cm an electric power of 1 W is required to keep the working temperature 1o °C above room temperature. The temperature distribution in the liquid crystal has a central region about 3 cm in diameter that is uniform to within o.1 °C; in a 1 cm thick surrounding ring the temperature then drops o.4 °C. Disadvantages of this heating method are that the foil and ring planes have to be adjusted parallel, and that setting the correct current value requires some effort.

With the use of metal absorption films much better heating facilities are now available: a heating current can be sent directly through the metal film. However, heating is only uniform if there are no cracks. This can easily be checked by measuring the resistance. The electrically supplied heat is lost essentially by radiative emission, theoretically with a power of o.oo6 W/cm^2 at an excess temperature of 1o°C. With the foil shown in Fig.1 1o V and 35 mA are in fact needed for setting the working point. At the boundary of the metallized region the gradients due to thermal conduction extend a few mm, the remainder of the 7 x 7 cm image area being uniform to within o.3 °C. The relaxation of the temperature follows the voltage and current changes with almost no inertia.

As the experiment showed, the metal film withstands a permanent electrical load of 4o V and 14o mA; this is equivalent to a power input of o.11 W/cm^2, which in vacuum according to the Stefan-Boltzmann law yields a temperature of 13o °C.

5. Coupling of Infrared Radiation and Read-Out System

The infrared radiation to be recorded impinges on the detector film through a vacuum-tight window. Vertical incidence is necessary for undistorted imaging. Furthermore, a large viewing angle, if possible the entire half-space, should be available for irradiation; this is particularly important for holographic observations. The window has therefore to be placed near (1 cm) the detector film. In particular, this allows the radiation to be manipulated very near to the detector. Only the opposite half-space therefore remains free for observing the colour phenomena in the liquid crystal film. Here also the line of observation is chosen perpendicular to the surface so as to avoid distortion. This can be done with a camera mounted on the outside of a glass window closing the vacuum vessel.

To complete the image converter, suitable white light illumination must be provided. Firstly, light from the infrared entry window has to be prevented from being transmitted through the liquid crystal film since the colour effects only appear in reflection. A remedy is afforded here by opaque windows made of germanium or black polythene. Secondly, the light used for illumination may not be reflected direct from the receiver surface (metal film) into the camera. This calls for oblique incidence.

In order to make the illumination uniform, an impractical large distance would be necessary with an ordinary flashlamp. On the other hand, the calculation for the above heating system shows that uniform illumination can be achieved in the near field of an annular source (See Figs. 2 and 3). This has the advantage that the flashlamp can be incorporated in the vacuum vessel without taking up too much room. The distance of the annular flash-lamp (lo cm in diameter) from the detector foil is 7 cm, so that a central field of view, 6.5 cm in diameter, is just free of direct reflections (Fig.5). The distance between liquid crystal film and camera lens is 26 cm.

With this geometry the illumination of the field of view is uniform, but the scattering angles vary. In the center of the image area the irradiation is incident uniformly at angles between 3o and 35 ^{o} to the normal, the line of observation being along the latter. For points 2.5 cm from the center of the image the line of observation is inclined 6 ^{o} to the normal, while the incidence angles vary between 26 ^{o} and 45 ^{o}, with the emphasis at 3o ^{o}. These angular differences have, however, surprisingly little effect on the observed colour. If the measurements of FERGASON /14/ are taken as a basis, the wavelength of the light scattered with maximum intensity should decrease by about 7o Å from the center of the image to a radius of 2.5 cm. This is roughly one-sixth of the distances between red, yellow, green, and blue. No red shift in the radial direction could in fact be observed.

The illumination time of the flashlamp, o.ool sec, is by a factor of 3 longer than the optimum delay time. It is sufficient for spatially resolving 5o line pairs per mm. The heating of the detector due to the flashlight is about o.1 ^{o} C, which can just be tolerated.

6. Assembly of the Liquid Crystal Image Converter

The liquid crystal detector was built on the principles already discussed, as shown in the scale drawing in Fig.5. The two detachable endplates of the vacuum vessel contain round apertures for infrared input and optical read-out. For photographing the submillimeter radiation a 2 mm thick Teflon window is used that bends a few mm under the influence of atmospheric pressure. The observation window is an 8 mm thick plexiglass sheet. The detector film and the illumination system are contained inside the vessel.

The vacuum vessel is connected direct to an electronically controlled oscilloscope camera (Steinheil Oszillophot M2), as shown in Fig.6. The camera is provided with a beam splitter for undistorted observation of the image by the experimenter. Permanent illumination is provided by four 1-Watt bulbs located on the in-

side wall of the vessel beside the annular flashlamp. This can be seen in Fig.7.

The frame with the detector foil (Fig.1) and, eventually, the heating ring (Fig.4) as well are attached to a rail rigidly mounted to the detachable endplate. The latter has vacuum-tight feedthroughs for the heating leads, and so assembling is very simple (Fig.8).

To ensure sharp imaging by the oscilloscope camera, the focal length of the objective has to be increased, e.g. by adding a dispersing lens. An image scale of 1 : 1 was considered suitable for observing the detector surface (6.5 cm diameter) because Polaroid films and 6 x 6 cm^2 colour films (Agfa CT 18) were used; therefore an 18 cm long tube was inserted between objective and film holder. Figure 9 shows the full field of view as seen on Polaroid film (Type 42).

7. Operation

The liquid crystal film is prepared by spraying the membrane with the substance dissolved in petroleum ether (Liquid Crystal Industries). If the film is heated in horizontal position to a temperature of about loo ^{o}C (by passing current through the metal film), the solvent quickly evaporates, leaving the cholesteric substance, which can order properly on cooling. The colour effect is then optimum. The film thickness can be found by weighing. Films kept at room temperature in closed containers still show good reaction after a number of weeks. Liquid crystal films that have become nonuniform can be washed off with petroleum ether.

The intensity of the flashlamp (Paffrath and Kemper UR 13o) requires an aperture of 11 or 16 with Agfa Color Film CT 18, and 16 or 22 with Polaroid Film Type 42. With apertures larger than 8 the image becomes blurred owing to the additional lens. Sufficient contrast can be achieved by mounting colour filters direct to the camera lens.

The camera can be opened by a trigger signal delivered by a laser pulse. For observation with longer infrared exposure times such as 1/5o sec use is made of a pulse generated when the infrared shutter closes. The camera stays open for 1/1oo sec. The firing of the flashlamp is delayed 1 msec after the camera is opened by a relay.

8. Photography with 337 µ Wavelength Radiation

First the liquid crystal image converter was tested by repeating previous experiments /16/ with a CO_2-laser (wavelength 1o.6 µ). Confirmation of the estimates in Section 3 was obtained, i.e. full contrast is achieved at an input energy density of o.oo4 J/cm^2, and the spatial resolution for an exposure time of 1/1oo sec is about 1o line pairs per mm. Furthermore, it was found by photographing 3oo nsec CO_2-laser pulses (see Section 2) that the detector can withstand a radiation power of at least 13 KW/cm^2 (equivalent to 2 KV/cm^2).

Far infrared radiation, which can best be produced at present by an HCN-laser at a wavelength of 337 µ (approximately o.1 W c.w.), has not been photographed hitherto with an image detector. The image converter described here now fills this gap /2o/. The value of such a detector is best illustrated by the following three experiments.

a) HCN-Laser Emission

For our first experiments we used a 6.5 m long HCN-laser with hole-coupling /21/; the liquid crystal image converter was placed 7o cm in front of the coupling mirror (see Fig.1o). Laser beam images photographed in this arrangement are shown in Figs. 11 - 14. They show a spot with a diameter of about 2 cm which, surprisingly, does not have rotational symmetric, monotonically decreasing power distribution. Instead, there are several maxima grouped in series at intervals of 3 to 6 mm. The power ratio between adjacent maxima and minima is about 2.

Before looking for an explanation of this distribution, we can determine the output power of the laser. The exposure time was o.3 to 1 sec, depending on the tuning of the laser. Estimating the area heated by o.5 ^{o}C to be 3 $\pm$ 1 cm^2, we obtain for the given sensitivity of the liquid crystal image converter, a total output power of 14 $\pm$ 5 mW or 45 $\pm$ 15 mW, depending on the tuning of the laser. The reflection and absorption losses due to the transmission through the 2 mm thick Teflon window of the detector were assumed to be 7 % and 5 % respectively.

In order to explain the observed power distribution, it is essential to consider the resonator modes. According to KOGELNIK and LI /22/ the hemispherical configuration (Fig.1o) has a confocal length b = 7.2 m, and a spot radius on the plane mirror and the concave mirror of w_o = 2 cm and 4.1 cm respectively; this shows that there can be no undisturbed TEM_{ooq} distribution. Near the concave mirror 1o % of the total power would be outside the laser tube; large variations due to reflection from the glass walls would therefore be expected here. STEFFEN and KNEUBÜHL /23/ have analyzed these influences and found, that the eigenfrequencies of the lowest "tube modes" are sufficiently different for only one of them to oscillate at a given resonator length. Furthermore, we observed resonator interferogramms similar to those obtained in /23/ with a Golay cell.

A look at the plane mirror of the resonator readily shows that the mode must be appreciably disturbed. About 52 % of the TEM_{ooq} mode would be coupled out through the hole, which is more than could be picked up by the amplifying system /24/. For laser oscillation to take place, the radiation distribution on the plane mirror has to be much wider than the Gaussian distribution characterized by w_o = 2 cm /25/. For this reason the relative amount of radiation impinging on the glass wall still exceeds the 1o % calculated for TEM_{ooq}. In addition, the intensity at the outer boundary of the plane mirror, i.e. 4.5 cm from the laser axis, will also rise above the value expected for TEM_{ooq} (which would be $2 \cdot 1o^{-5}$ relative to the axis value).

We are thus on the way to explaining the structure observed in Figs. 11 - 14: it represents the interference pattern which is induced in the laser beam emerging from the central aperture by the radiation emitted around the mirror edge. A beam emanating from the outer boundary of the mirror intersects the laser axis in the image plane at an angle of 4.5/7o = 64 mrad, thus producing interference fringes with a separation of o.337/o.o64 = 5.3 mm. The superposition of many such beams gives rise to the patchy structure observed. The structure does not show rotational symmetry because the mirrors are not aligned exactly perpendicular to the tube axis. It follows from the intensity ratios that even at a distance of very few mm from the tube wall the power density of the mode is still several per cent of the maximum.

It should be worthwhile using the liquid crystal image converter for systematically studying the radiation distribution in submillimeter wave lasers. This would afford another means of testing "tube modes" /23/ in the cases of hole coupling and metal mesh coupling.

b) Two-Dimensional Interferograms at 337 /u

To prevent the interference fringes from having too large a separation $d = \lambda/2\sin\varepsilon/2$, the angle ε between the reference and object beams in the case of submillimeter radiation should be at least a few degrees. The simple interferometer shown in Fig.15 was chosen. A Fresnel biprism made of Teflon was used to produce interference between the two halves of the beam. The resulting interferogram is shown in Fig.16. It gives a fringe distance of $1.8 \pm o.1$ mm. Given the 14.5° angle of refraction α of the prism, the refractive index of Teflon is found to be $1.37 \pm o.o3$. Other optical components of Teflon were made for use in interferometric measurements of the electron density distribution in plasmas. Figure 17 shows the focal line of a cylindrical lens with a radius of curvature of 5 cm (focal distance approximately 11 cm). A brief estimate shows that the diffraction limited focal width of 2 mm is obtained.

c) Focusing with Conical Waveguides

Conical waveguides made of metal are used in experiments with HCN-laser radiation to concentrate the radiation on a detector element. In particular, this is intended to compensate small directional fluctuations of the incoming beam. Our pictures show how strongly structured the radiation is at the outlets of such waveguides, and how sensitive the structure is to small changes of angle.

Figure 18 was obtained 17 mm after the outlet of a cone roughly wrapped from silver paper with inlet aperture 3 cm in diameter, length 4o cm and outlet aperture o.5 cm in diameter. The cone half-angle here was 2.2 °.

The second cone had twice as large an apex angle and was made of polished brass. The inlet aperture was 4 cm in diameter, the length 2o cm, and the outlet aperture 1 cm in diameter. For the picture sequence in Figs. 19 - 22 the cone was fixed at its inlet aperture and swivelled through small angles up to 6 °. The pictures are again taken 17 - 19 mm from the outlet aperture. It can be seen that of an angle of about 3 ° (i.e. when the rays have been reflected from the wall once on the average) the radiation distribution assumes certain symmetries that are reminiscent of waveguide modes. At an angle of incidence of 5.5 ° (Fig.19) the main direction of emission is inclined 2o ° to the axis of the cone.

9. Applications

The liquid crystal image converter allows the experimental physicist working with laser radiation in the infrared and submillimeter wavelength regions to use photographic reception techniques. The 33 cm^2 large detector field available in the described image converter can be used for recording two-dimensional intensity distributions (imaging) or one-dimensional intensity distributions as functions of time (streak pictures, oscillograms). As the image conversion effect involved is reversible,

the pictures can be taken at intervals of the thermal equalization time of a few seconds. Obvious applications are possible in the following two fields:

a) Laser Physics

As was shown above in the case of the HCN-laser, the liquid crystal image converter allows investigation of the forms of emission and mode structures of infrared lasers. Such analyses should be important mainly for chemical lasers and transversely pulsed lasers in which the gain distribution is highly non-uniform. Furthermore the radiation intensity is absolutely determined, without special calibration and irrespective of wavelength. Time resolution can be achieved by one-dimensional focusing and smearing perpendicular to the line of focus with a rotating mirror. The practicable resolution limit can be estimated by taking about 1ooo Hz as rotation frequency and 1 m as the distance between rotating mirror and image detector; one microsecond is then displayed over a length of 1.3 cm. With the spatial resolution of 1oo line pairs per mm this yields an ultimate time resolution of o.8 nsec.

b) Plasma Physics

In plasma physics the liquid crystal image converter allows measurements of electron density distributions, time resolved under certain circumstances. As explained at the outset, infrared and submillimeter wavelength radiation is required for selective measurement of the electron density. The shortest possible exposure times are governed by the sensitivity of the liquid crystal image converter (o.oo4 J/cm^2) and the power of the laser involved, viz. $1o^{-9}$ sec at a wavelength of 1o μ (TEA-CO_2-laser) and $1o^{-5}$ sec at 337 μ (pulsed HCN-Laser).

Besides phase shift (interferometry), other effects associated with transmission through a plasma can be used for measurement, such as absorption, beam deflection and Faraday rotation. All these changes can, in principle, be observed from a suitably exposed holographic picture. In fact, with the spatial resolution of 1oo line pairs per mm it is possible to make holograms for wavelengths longer than about 1o μ.

lo. Acknowledgments

The author wishes to thank Mr. F. Komenda and Mr. H. Zinkl for constructing the detector and Dr. K.F. Renk for contributing to the measurements with the HCN-laser.

11. References

/1/ F. Keilmann, Possibilities for Plasma Diagnostics with Infrared Lasers, Rep. IPP 3/98, Institut für Plasmaphysik, Garching (1969)

/2/ A.R. Laufer, Editor, Proc. IRE 47, 1415 - 1649 (1959)

/3/ O.A. Zinovev, On a Method of Investigating Electromagnetic Waves, Sov. Phys. JETP 25, 752 - 754 (1967)

/4/ H. Inaba, T. Kobayashi, K. Yamawaki, and A. Sugiyama, Direct Observation of Output Beam Patterns from N_2-CO_2 Laser at lo.6 μ by Thermal Development Method, Infr. Physics 7, 145 - 149 (1967)

/5/ T. Izawa and M. Kamiyama, Infrared Holography with Organic Photochromic Films, Appl. Phys. Letters 15, 2ol - 2o3 (1969)

/6/ J.S. Chivian, R.N. Clayton, and D.D. Eden, Infrared Holography at lo.6 μ, Appl. Phys. Letters 15, 123 - 125 (1969)

/7/ D. Meyerhofer, Measurement of the Beam Profile of a CO_2 Laser, IEEE J. Quantum Electronics QE-4, 969 - 97o (1968)

/8/ M. Czerny, Über Photographie im Ultraroten, Z. Physik 53, 1 - 12 (1929)

/9/ G.W. McDaniel and D.Z. Robinson, Thermal Imaging by Means of the Evaporograph, Appl. Optics 1, 311 - 324 (1962)

/lo/ K. Iizuka, Microwave Holography by Means of Optical Interference Holography, Appl. Phys. Letters 17, 99 - lol (197o)

/11/ F. Urbach, N.R. Nail, and D. Pearlman, The Observation of Temperature Distributions and of Thermal Radiation by Means of Non-Linear Phosphors, J. Opt. Soc. Amer. 39, lo11 - lo19 (1949)

/12/ A.I. Carlson, Transient Temperature Response of Thin Film Thermal Detectors in Infrared Imaging Systems, Appl. Optics 8, 243 - 253 (1969)

/13/ J.R. Hansen, J.L. Fergason, and A. Okaya, Display of Infrared Laser Patterns by a Liquid Crystal Viewer, Appl. Optics 3, 987 - 988 (1964)

/14/ J.L. Fergason, Liquid Crystals in Nondestructive Testing, Appl. Optics 7, 1729 - 1737 (1968)

/15/ C.F. Augustine, C. Deutsch, and D. Fritzler, Microwave Holography Using Liquid Crystal Area Detectors, Proc. IEEE 57, 1333 - 1334 (1969)

/16/ F. Keilmann, Infrared Interferometry with a CO_2 Laser Source and Liquid Crystal Detection, Appl. Optics 9. 1319 - 1322 (197o)

/17/ D.W. Berreman and T.J. Scheffer, Bragg Reflection of Light from Single-Domain Cholesteric Liquid-Crystal Films, Phys. Rev. Letters 25, 577 - 581 (197o)

/18/ H. Murmann, Untersuchungen über die Durchlässigkeit dünner Metallschichten für langwellige ultrarote Strahlung und ihre elektrische Leitfähigkeit, Z. Physik 54, 741 - 76o (1929)

/19/ L.N. Hadley and D.M. Dennison, Reflection and Transmission Interference Filters, J. Opt. Soc. Amer. 37, 451 - 465 (1947)

/2o/ F. Keilmann and K.F. Renk, Visual Observation of Submillimeter Wave Laser Beams, Appl. Phys. Letters 18, 452 (1971)

/21/ J.P. Kotthaus, Submillimeter-Gaslaser für kontinuierlichen und Q-Schaltungs-Betrieb und hochauflösende EPR-Spektroskopie bei $1o^{12}$ Hz, Diplomarbeit TH München, Teilinstitut Dransfeld (1968)

/22/ H. Kogelnik and T. Li, Laser Beams and Resonators, Appl. Optics 5, 155o (1966)

/23/ H. Steffen and F. K. Kneubühl, Resonator Interferometry of Pulsed Submillimeter-Wave Lasers, IEEE J. Quantum Electronics QE-4, 992 - 1oo8 (1968)

/24/ R. Ulrich, T.J. Bridges and M.A. Pollack, Variable Metal Mesh Coupler for Far Infrared Lasers, Appl. Optics 9, 2511 - 2516 (197o)

/25/ D.E. McCumber, Eigenmodes of a Symmetric Cylindrical Confocal Laser Resonator and Their Perturbation by Output Coupling Apertures, Bell. Sys. Tech. J. 44, 917 - 932 (1965)

/26/ M. Yamanaka, H. Yoshinaga and Shozo Kan, Time Behaviour of Pulsed Output, Transverse Mode Pattern and Polarization Characteristics in Far Infrared CN Lasers, Jap. J. Appl. Physics 7, 25o - 256 (1968)

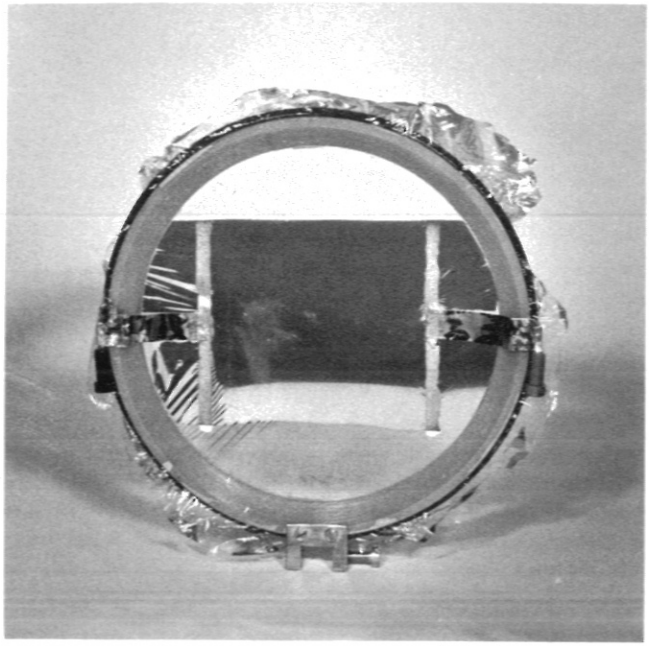

Fig. 1

Hostaphan foil with dully reflecting chromium coating

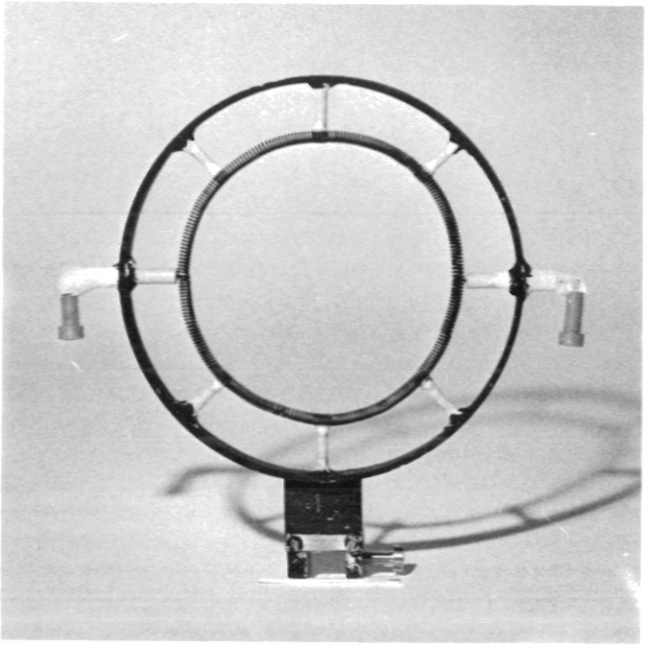

Fig. 4

Heating ring

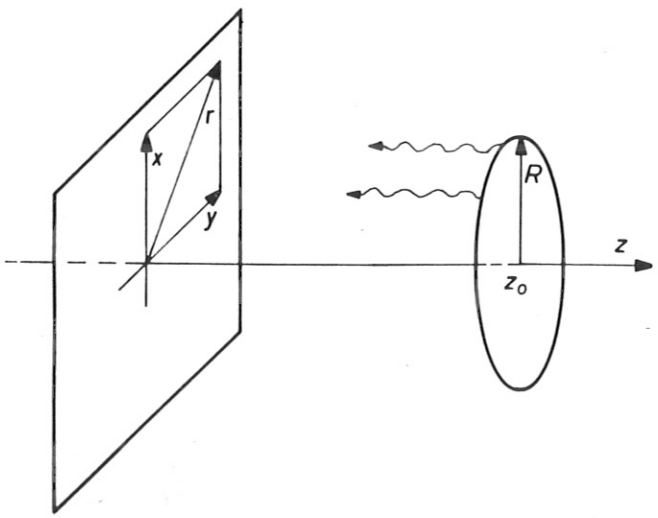

Fig. 2

Emission of an annular source

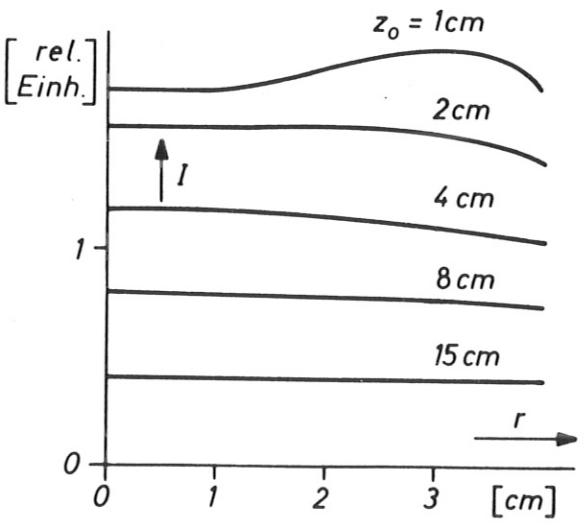

Fig. 3

Irradiation profiles for an annular source at a distance of z_o

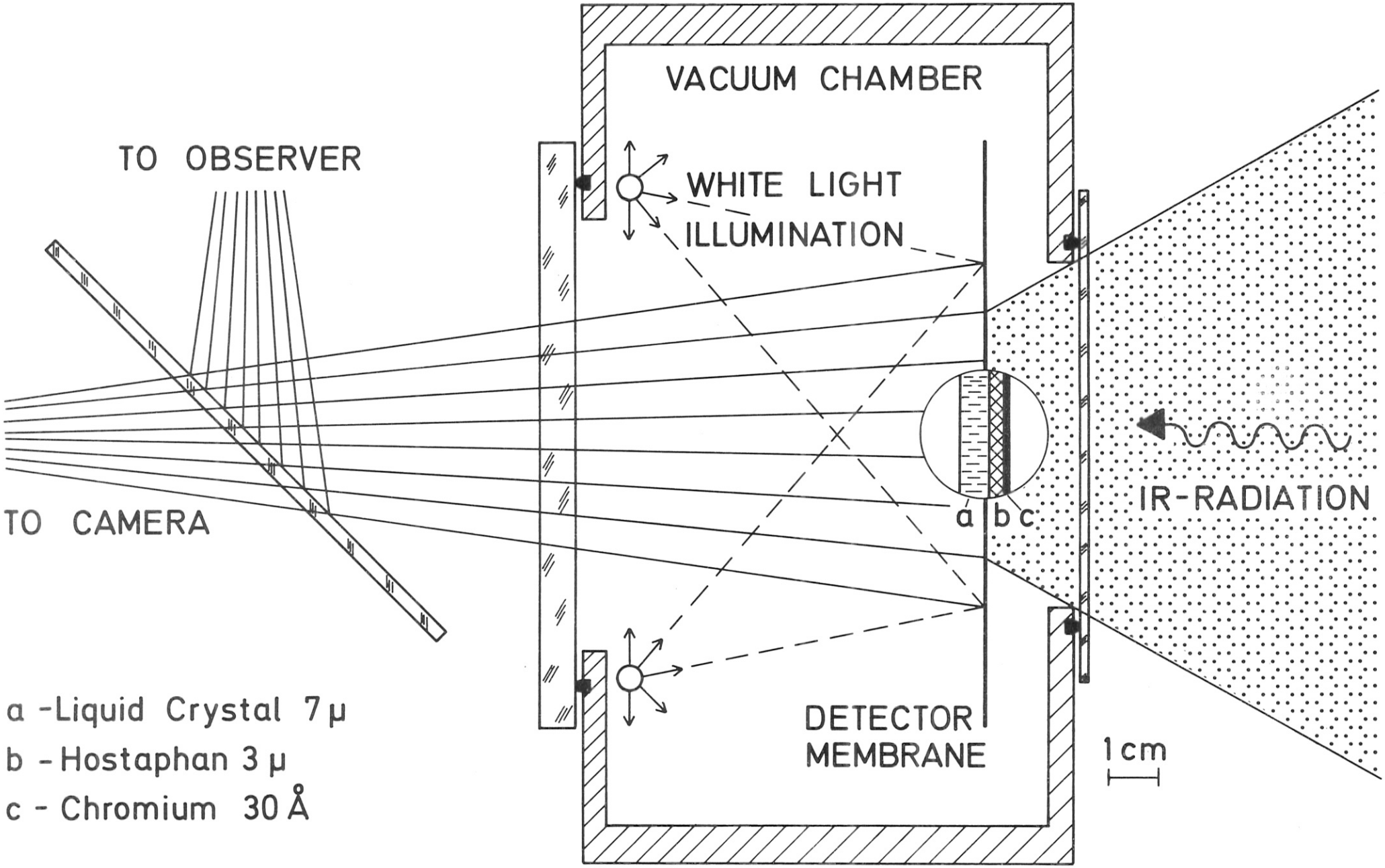

Fig.5 Design of the image detector

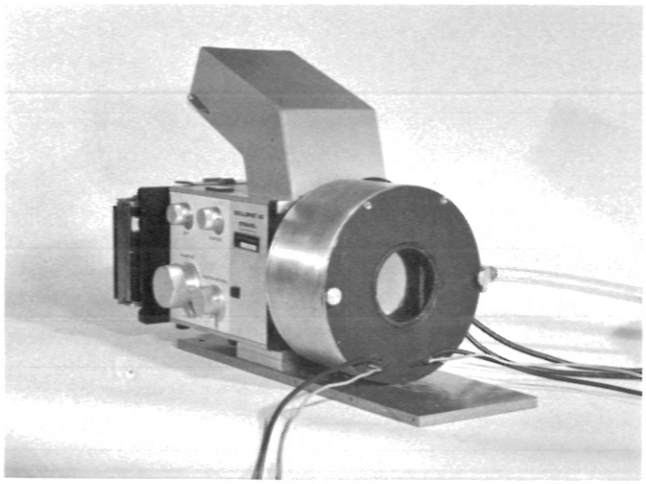

Fig. 6

Image detector,
infrared window removed

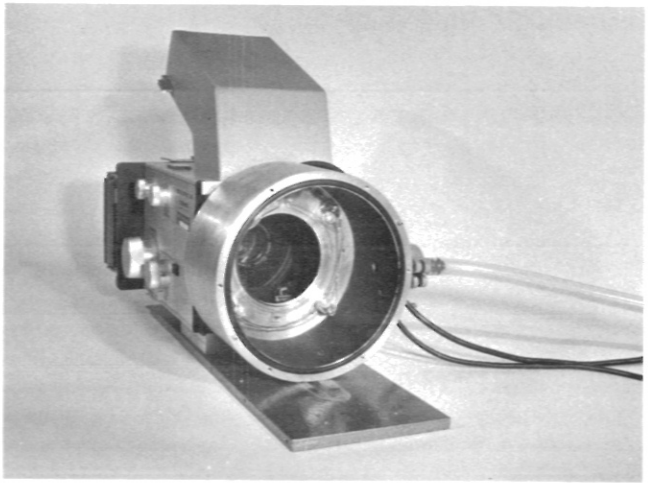

Fig. 7

Image detector,
rear panel removed

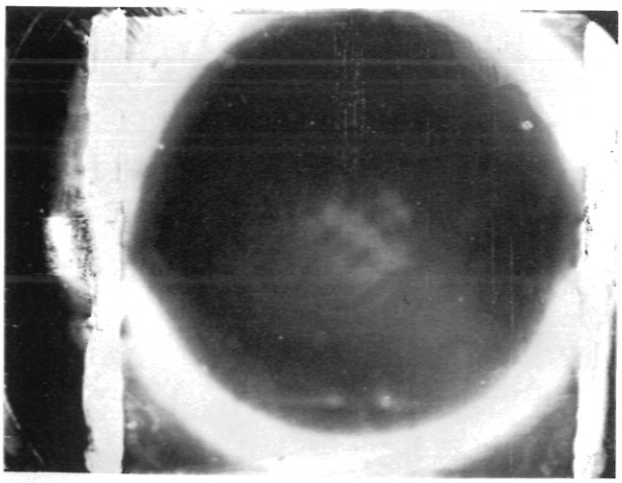

Fig. 9

Field of view for Polaroid
Type 42, size 72 x 95 mm^2

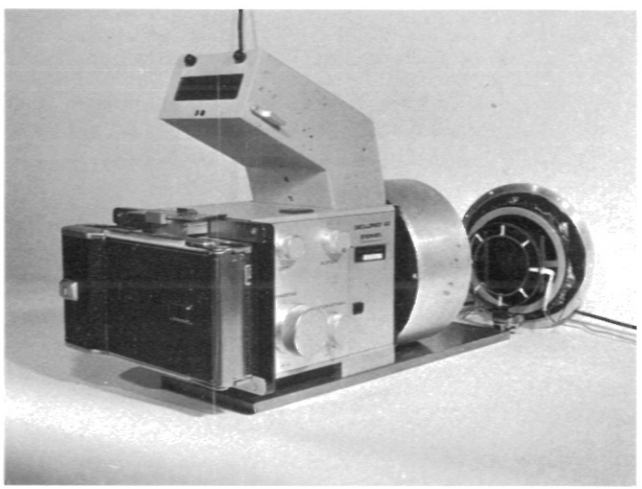

Fig. 8

Image detector

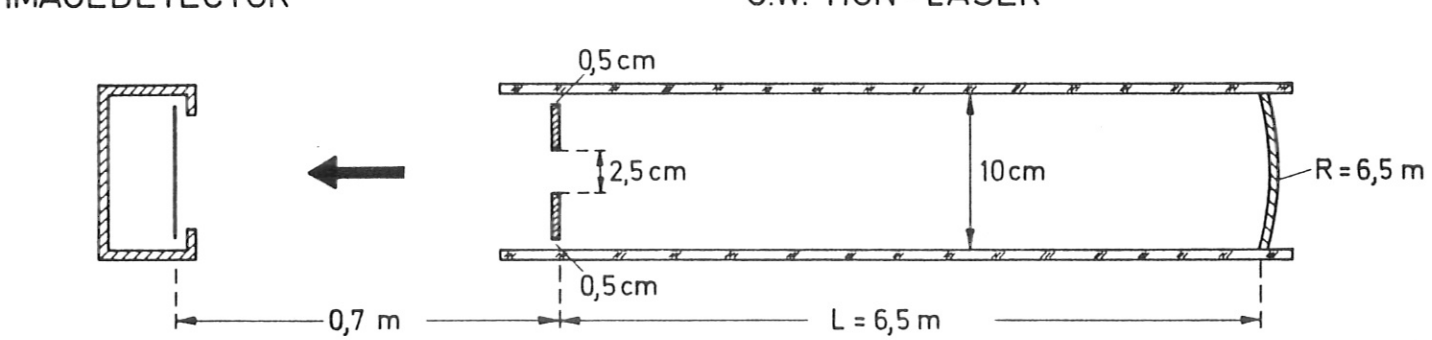

Fig.1o Experimental set-up for photographing HCN-laser emission

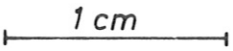

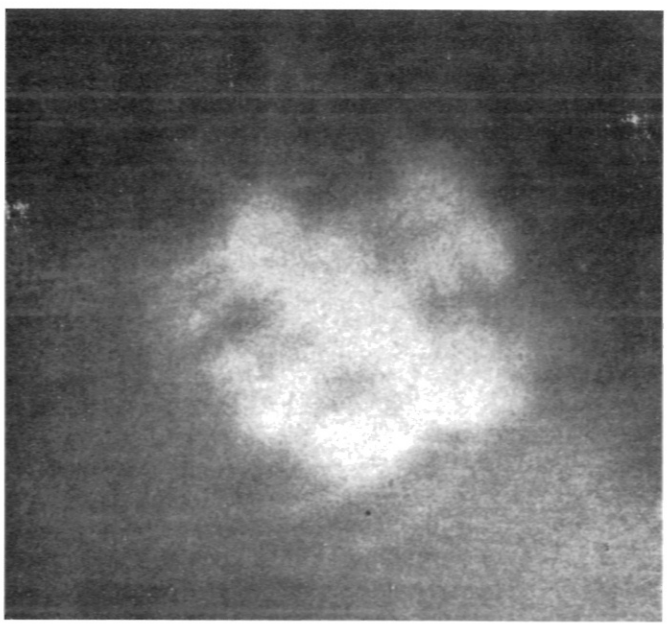

Fig.11 Output beam pattern of HCN-laser

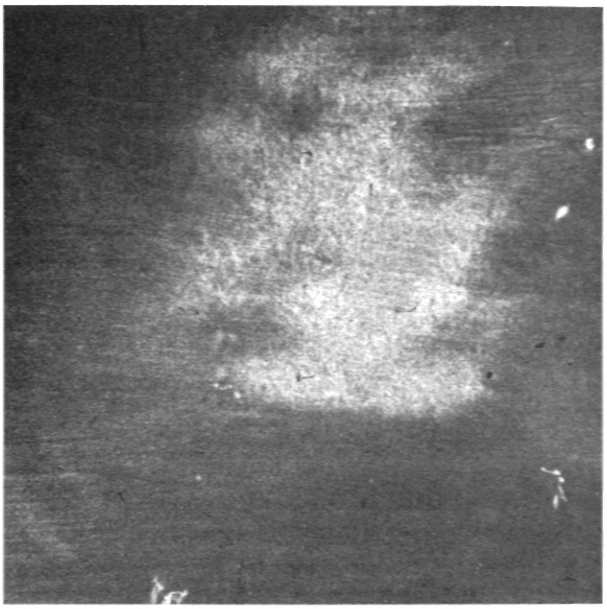

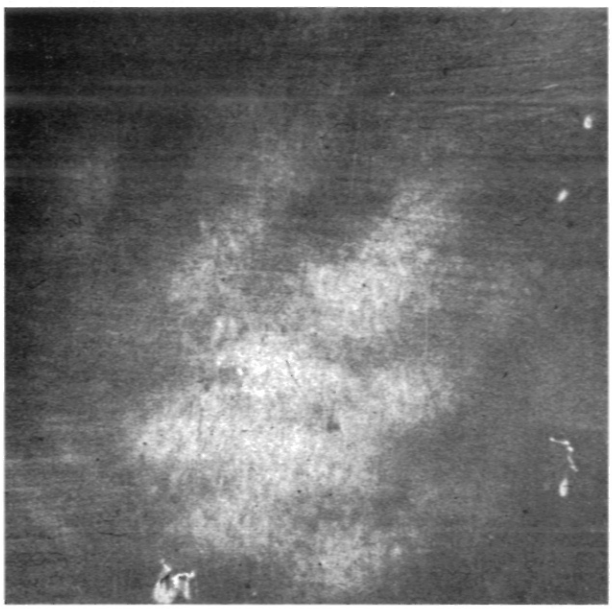

1 cm

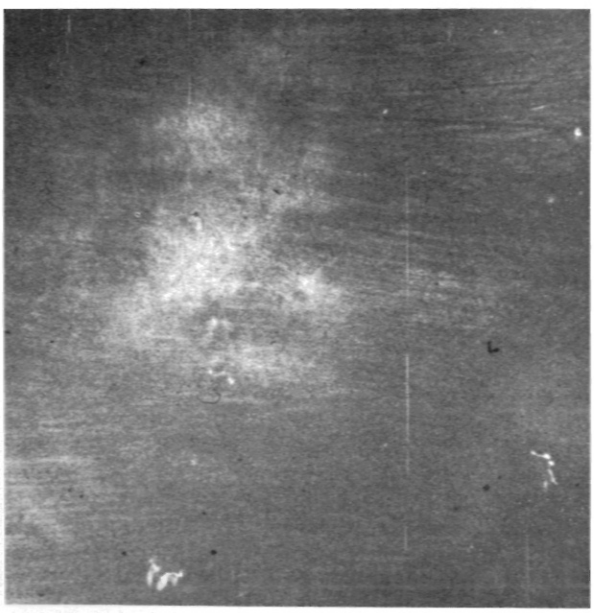

Figs. 12 - 14

Output beam patterns of HCN-laser

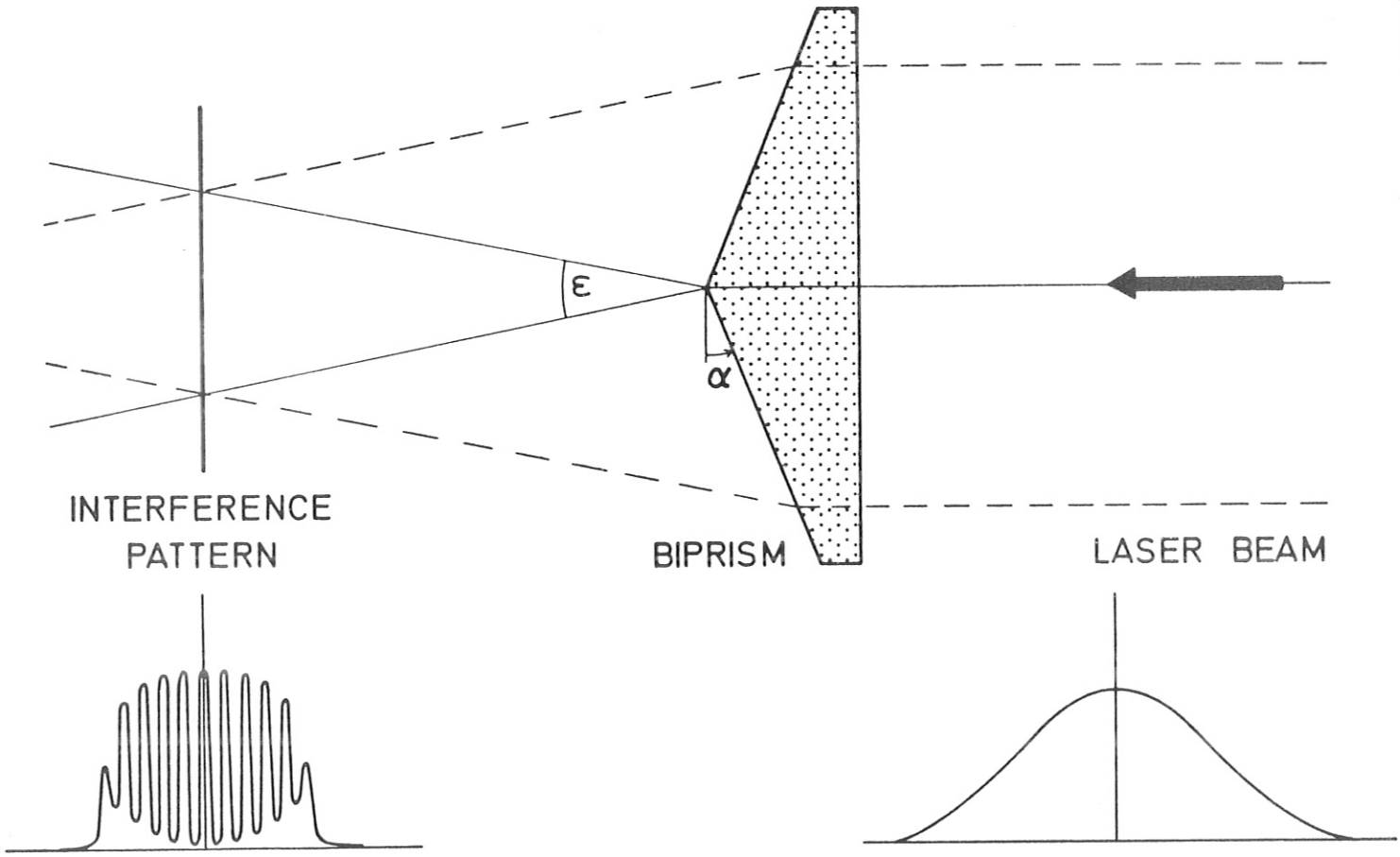

Fig.15 Sketch of Fresnel interferometer

Fig. 16

Interferogram at 337 μ; fringe separation 1.8 mm

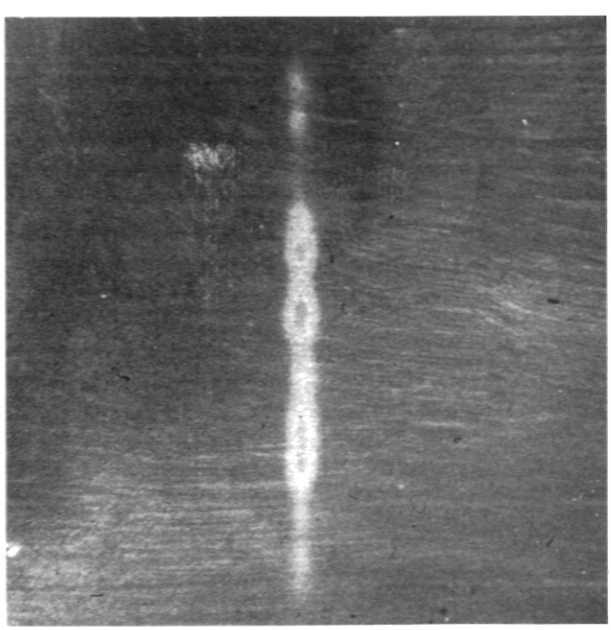

Fig. 17

Focal line of a cylindrical lens for 337 μ radiation

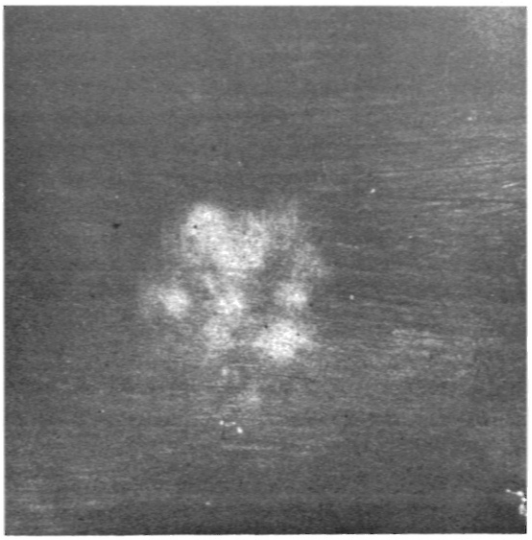

Fig.18 Beam structure at outlet of cone made of silver paper

$\alpha = 5,5^{\circ}$

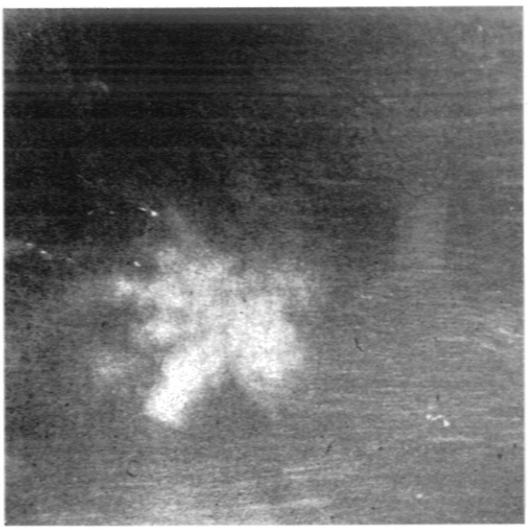

$\alpha = 3,5^{\circ}$

$\alpha = 1^{\circ}$

$\alpha = 4,5^{\circ}$

Figs. 19 - 22 Beam structure at outlet of brass cone with its axis inclined at an angle α to the beam direction